Applied Environmental Research
- RESEARCH FOR SUSTAINABLE PLANET -

Research Article

Efficient Oxidation of Methylene Blue via Catalytic Activation of Peroxymonosulfate via an Engineered δ-FeOOH/Pili Nutshell Biochar Composite

Lorenz E. Borromeo

Department of Environmental and Sanitary Engineering, Technological Institute of the Philippines, Quezon City, Metro Manila, Philippines

*Corresponding Email: lborromeo.ense@tip.edu.ph

Abstract

This study introduces a novel composite catalyst formed by anchoring delta iron oxyhydroxide (δ-FeOOH) onto pyrolyzed Pili nutshell biochar via a room-temperature coprecipitation technique, marking the first application of Pili nutshell waste in advanced oxidation processes for wastewater treatment. This innovative methodology enhances catalyst dispersion and stability, facilitating the activation of peroxymonosulfate (PMS) to generate reactive sulfate radicals ($SO_4^{\bullet-}$) for the degradation of methylene blue (MB), a thiazine dye commonly used in the medical field and the dye industry. Different techniques have been used to characterize synthesized composites in terms of their morphology, elemental composition, surface functional groups, and crystalline phase structure. The system achieved a maximum MB degradation efficiency of 90.88% within 30 min at pH 6.0 when low dosages of PMS and the δ-FeOOH/biochar composite were used, following pseudo-first-order degradation kinetics. Radical scavenging experiments confirmed that $SO_4^{\bullet-}$ radicals were primarily responsible for the degradation process. Notably, the composite maintained over 70% removal efficiency after four reuse cycles, indicating its potential for sustainable and cost-effective wastewater treatment. This research highlights the effectiveness of the δ-FeOOH/biochar/PMS system as a promising solution for treating MB-laden wastewater, contributing to environmental sustainability and waste valorization.

ARTICLE HISTORY

Received: 5 Oct. 2024
Accepted: 11 Feb. 2025
Published: 10 Mar. 2025

KEYWORDS

Biochar;
Iron oxyhydroxide;
Methylene blue;
Peroxymonosulfate;
Pili nutshell

Introduction

Methylene blue (MB) ($C_{16}H_{18}N_3SCl$) is a synthetic dye that has been widely used in medical and biological applications [1]. However, when MB-laden wastewater is released without proper treatment or regulation, it can have several adverse effects, such as aquatic pollution, soil contamination, and groundwater contamination. The sulfate radical-based advanced oxidation process (SR-AOP) is a new, advanced, and highly efficient technique for the treatment of organic contaminants. Peroxymonosulfate (PMS) (HSO_5^-) is commonly employed to generate highly reactive sulfate radicals ($SO_4^{\bullet-}$) through various activation processes. Compared with hydroxyl radicals ($^{\bullet}OH$), $SO_4^{\bullet-}$ radicals offer high reactivity, longer half-lives, and selective degradation of a wide range of organic contaminants [2]. Notably, delta iron oxyhydroxide (δ-FeOOH) has been widely investigated and has demonstrated remarkable efficiency as a single-phase catalyst for various applications, including PMS activation, as it aids in electron transfer, surface reactions, and redox cycling [3]. Furthermore, δ-FeOOH is known for its stability under various environmental conditions, which can lead to a longer lifespan of the catalyst in repeated use scenarios. This stability is crucial for practical applications where catalyst regeneration is often a challenge [4]. However, a major drawback of δ-FeOOH is its agglomeration due to its intrinsic magnetic properties. The incorporation of δ-FeOOH into the biochar (BC) matrix can significantly enhance the activation of PMS. Carbon-based support materials such as agro-industrial waste-

https://doi.org/10.35762/AER.2025006

derived BC can decrease particle agglomeration and offer exceptional adsorptive properties owing to their porous structure and the presence of charged oxygenated surface functional groups [5]. This modification may improve electron transfer processes, leading to more efficient oxidation reactions than unmodified BC or other metal oxides used in similar studies.

Pili nut (*Canarium ovatum*) is a fruit native to the Philippines, where it is a significant agricultural product, with the country being the only commercial producer. The Bicol Region, especially the mountainous areas of Sorsogon, Albay, and Camarines Sur, leads in Pili nut production. The annual yield averages 7,400 MT, with a peak of 8,200 MT in 2013 [6]. However, the shells of Pili nuts are underused agricultural waste. By turning waste into a useful resource, the use of these shells to produce BC helps with waste management and promotes sustainable practices [7–8]. In addition, a BC with a desirable balance of functional groups that improve reactivity and stability in catalytic processes may be produced by pyrolyzing waste Pili nutshells. Pili nutshell-derived BC has been extensively studied for its potential as an adsorbent for toxic gas and small liquid molecules because of its high lignocellulosic content, large BET surface area, and microporous structure. These characteristics might provide a competitive edge in catalytic applications, as they differ greatly from those of other biomass sources [9]. In a study by Yao et al. in 2015 [10], pyrolyzed BC derived from Pili nutshells exhibited superior adsorption capabilities due to its unique porous structure and high surface area, which could exceed 817.19 $m^2\ g^{-1}$. This quality is necessary for the efficient removal of pollutants, such as MB. Although the adsorption properties of Pili nut shells have been investigated, there is a noticeable lack of information about their use in advanced oxidation processes.

In this study, a novel carbocatalyst made from pyrolyzed waste Pili nutshells impregnated with δ-FeOOH particles (δ-FeOOH/BC) was synthesized to activate PMS to remove MB in aqueous solution. The objectives of this study are to (i) synthesize and characterize a δ-FeOOH/BC catalyst prepared by slow pyrolysis of waste Pili nutshells followed by room-temperature coprecipitation of $FeCl_3$•$6H_2O$ using NaOH; (ii) perform heterogeneous activation of PMS via the prepared δ-FeOOH/BC as a catalyst for MB removal; (iii) investigate the effects of catalyst dosage, PMS dosage, and solution pH on MB removal; and (iv) carry out catalyst recyclability experiments and radical quenching experiments to assess the stability of the composite and identify the dominant radicals responsible for MB degradation.

Materials and methods

1) Materials and reagents

All the chemicals were of reagent grade and were used as received without further treatment and purification. Waste Pili nut shells were supplied by a local Pili nut confectionery in Albay, Philippines. Methylene blue hydrate ($C_{16}H_{18}N_3SCl$•XH_2O, 100%) and potassium peroxymonosulfate ($KHSO_5$, 100%) were obtained from Sigma–Aldrich, Singapore. Ferric chloride hexahydrate ($FeCl_3$•$6H_2O$, ≥97%) was procured from Loba Chemie, India. Anhydrous ethyl alcohol (C_2H_5OH, 99.5%) was purchased from Chem-Supply Pty Ltd., Australia. Anhydrous tert-butyl alcohol ($(CH_3)_3COH$, 99.5%), sodium hydroxide pellets (NaOH, ≥98%), and concentrated hydrochloric acid (HCl, 37%) were purchased from DKL Laboratory Supplies, Philippines. All the solutions used in the experiments were prepared with deionized water (DI, 16 MΩ).

2) Synthesis and characterization of BC, δ-FeOOH, and the δ-FeOOH/BC composite

Waste Pili nutshells were cleaned with DI water to eliminate any adhered dirt or other macro impurities. The shells were then ground manually to obtain a 5–10 mm size and subjected to slow pyrolysis at 450 °C for 3 h in an air-limited muffle oven (Vulcan A-550, USA) to produce BC. After that, it was pulverized via a domestic electric grinder and passed through a 200-mesh Tyler sieve. The composite catalyst was prepared at room temperature following the coprecipitation method generally described by Threepanich and Praipipat [11]. Typically, 3.0 g of $FeCl_3$•$6H_2O$ and 1.0 g of prepared BC were magnetically stirred (Corning PC-420D, USA) in 100 mL of DI water for 3 h to ensure complete dispersion. Then, 5% (m/v) NaOH was added dropwise to the Fe-BC mixture to facilitate the deposition of δ-FeOOH particles onto the surface, as shown in Eqs. 1 and 2.

The reaction pH was controlled until it reached ≈10 (Horiba LAQUA PH1100, Singapore). Finally, the prepared composite was vacuum-filtered, washed several times with DI water, and oven-dried (Memmert U-30, UK) for 48 h at 80 °C. The preparation of pure δ-FeOOH particles was accomplished by employing the same procedure without the incorporation of BC.

$$BC + FeCl_3 \bullet 6H_2O \rightarrow BC \bullet Fe^{+3} + 3Cl^- + 6H_2O \quad \text{(Eq. 1)}$$

$$BC \bullet Fe^{+3} + 3Cl^- + 3NaOH \rightarrow BC \bullet FeOOH + 3NaCl + H_2O \quad \text{(Eq. 2)}$$

A scanning electron microscope (TM4000Plus II Hitachi, Japan) equipped with an energy-dispersive X-ray detector (Xplore Compact 30 Oxford, UK) at an accelerating voltage of 15.0 kV was used to examine the morphology and elemental composition of the as-prepared catalysts. X-ray diffraction (MAXima XRD 7000 Shimadzu, Japan) using a CuK_α radiation source at 40.0 kV and 30.0 mA with a wavelength of 1.54 Å was used to verify the crystalline phases. Diffraction patterns formed by X-ray beams were collected over the 2θ range of 10–70°. To identify the surface functional groups and bond formations, the δ-FeOOH/BC sample was subjected to Fourier transform infrared spectroscopy-attenuated total reflectance (UV-1700 Shimadzu, Japan) over wavenumbers ranging from 600–4,000 cm^{-1}.

3) Methylene blue removal experiments and analytical methods

Batch adsorptive and catalytic degradation experiments were performed for each synthesized material. In separate vessels, 25 mg of each powdered sample (BC, δ-FeOOH, δ-FeOOH/BC) was mixed with 100 mL of 30 mg L^{-1} synthetic MB solution and allowed to adsorb for 30 min at 350 rpm at 25 °C. In a separate setup, 0.4 g L^{-1} PMS was added to each flask to catalytically degrade MB following the previous MB concentration and mass of powdered samples. All treatment solutions were adjusted to pH 6 via NaOH or HCl for both experimental setups. Every 5 min, 2 mL of sample mixture was extracted, filtered through a 0.45-μm PVDF filter, and analyzed for the residual MB concentration. The influences of different parameters, namely, the solution pH (2.0–10.0), catalyst dosage (0.050–0.450 g L^{-1}), and PMS dosage (0.1–0.7 g L^{-1}), on the removal of MB were studied. The catalyst recyclability experiments were performed under the optimized conditions to assess the efficiency of the catalyst after five consecutive cycles. Finally, radical quenching experiments were performed to identify the dominant radicals responsible for MB degradation. The exact procedures of degradation were followed, except for the addition of 0.1 M $(CH_3)_3COH$ and 0.1 M C_2H_5OH as quenching agents for $^{\bullet}OH$, and $^{\bullet}OH$ and $SO_4^{\bullet-}$, respectively.

For each run, the residual concentration of MB was analyzed via ultraviolet–visible spectroscopy (Hitachi UH-5300, Japan). The maximum absorption wavelength of the 30 mg L^{-1} MB solution was set at 665 nm after a spectral scan was performed. The removal efficiency R (%) was calculated via Eq. 3. All the measurements were carried out in duplicate.

$$R\ (\%) = \frac{C_i - C}{C_i} \times 100 \qquad \text{(Eq. 3)}$$

where R (%) refers to the amount of MB removed and C_i (mg L^{-1}) and C (mg L^{-1}) represent the initial and final concentrations of MB after the treatment, respectively.

4) Determination of degradation kinetics

The MB degradation performance of the different treatment systems was fitted via linear regression analysis via both a pseudo-first-order kinetic model and a pseudo-second-order kinetic model, as shown in Eqs. 4 and 5:

$$-\ln\left(\frac{C}{C_i}\right) = k_{obs}t \qquad \text{(Eq. 4)}$$

$$\frac{1}{C} = k_{obs}t + \frac{1}{C_i} \qquad \text{(Eq. 5)}$$

where C_i is the initial concentration of MB (mg L^{-1}), C is the final concentration of MB at any time t (mg L^{-1}), and k_{obs} is the corresponding kinetic constant for MG degradation. The coefficient of determination (R^2) was used to assess the model's goodness-of-fit. The model with the highest R^2 value was considered the best representation of the degradation kinetics.

Results and discussions

1) Characterization

The morphologies of BC, δ-FeOOH, and δ-FeOOH/BC are shown in Figures 1 (a–c). The prepared BC exhibited irregular fine pores in its internal structure, which could increase the contact surface area for δ-FeOOH adhesion and MB adsorption. Moreover, the pure δ-FeOOH particles were observed to have a typical cubic morphology with distinct mesoporous aggregations, as shown in Figure 1(b). This structure is inherent to δ-type FeOOH particles, as observed in the 2015 study of different phases of FeOOH by Mei and colleagues [12]. Effective adhesion and dispersion of the δ-FeOOH particles were observed on the BC surface, as shown in Figure 1(c). As shown in Figure 1(d), C, O, and Fe were detected in the as-prepared δ-FeOOH/BC composite, confirming the successful incorporation of δ-FeOOH into BC. The trace amount of Si might be due to the Si-Li detector on the mounting base of the equipment used in the analysis [13]. The presence of Na and Cl came from the NaOH and HCl used during synthesis, whereas the presence of Au originated from the gold sputtering pretreatment conducted before the sample was subjected to electron microscopy.

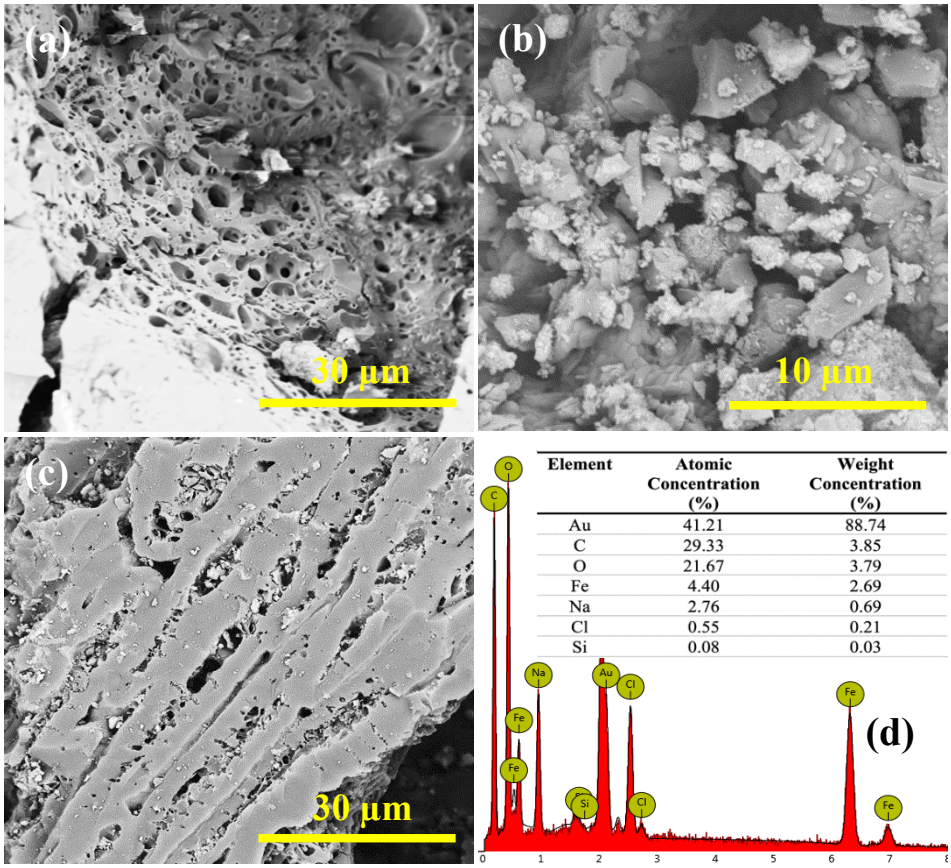

Element	Atomic Concentration (%)	Weight Concentration (%)
Au	41.21	88.74
C	29.33	3.85
O	21.67	3.79
Fe	4.40	2.69
Na	2.76	0.69
Cl	0.55	0.21
Si	0.08	0.03

Figure 1 Electron micrographs of (a) BC, (b) δ-FeOOH, (c) δ-FeOOH/BC composite and (d) EDX spectrum of the δ-FeOOH/BC composite (inset: elemental composition in percent atomic and weight concentration).

Infrared spectroscopy analysis revealed numerous peaks, confirming the presence of different functional groups on the composited catalyst surface, as shown in Figure 2(a). The broad peak at 3,300 cm^{-1} can be indexed to the –OH group [14], whereas the sharp peak at 1,634 cm^{-1} can be related to the C=O group [15]. Moreover, the bending vibration of C–H could be attributed to the peaks at 2,200 cm^{-1} and 1,400 cm^{-1} [16]. The bending and stretching vibrations of Fe–O–H could be associated with peaks at 1,120 cm^{-1} and 880 cm^{-1} emanating from the bonding of Fe and BC [17].

In Figure 2(b), the synthesized BC, δ-FeOOH, and δ-FeOOH/BC composites were compared with standard graphitic carbon and δ-FeOOH diffractograms obtained elsewhere [18]. The amorphous and graphitic structure of BC was confirmed by the presence of a broad peak at 23.52° and some obscure representative peaks at 43.19° and 60.01° [19]. After synthesis, the successful adhesion of δ-FeOOH on BC was confirmed by conspicuous peaks reflected at 34.83°, 40.60°, 54.52°, and 63.28°, which represent the (100), (101), (102), and (110) planes, respectively. δ-FeOOH particles were likely formed on the surface of BC, explaining why the majority of the diffraction peaks related to δ-FeOOH remained unchanged in the composited catalyst. The formation of a trace quantity of α-FeOOH on the prepared δ-FeOOH particles was observed, as confirmed by small peaks at 21.36° and 59.3°. Fe^{+3} may substitute for the isoforms during crystal formation, leading to distinct phases of FeOOH. Thus, a mixed form of FeOOH may exist because of its comparable crystallization profile. A similar scenario was observed in the work of Tavares and colleagues in 2020 [20]. Fortunately, these peaks noticeably disappeared in the final composited sample, which was attributable to possible unit cell distortion and structural transformation of the δ-FeOOH/BC. Overall, both the FTIR and XRD results confirmed the successful synthesis of the δ-FeOOH/BC composite.

2) Batch MB adsorption and degradation in different systems

As shown in Figure 3, the adsorption performance of the synthesized catalysts was minimal and was not the primary mechanism of removal. BC only showed ~17% removal due to possible electrostatic repulsion of MB on its surface sites. Moreover, the δ-FeOOH particles demonstrated a relatively lower removal efficiency of ~14%. This could be attributed to the evident magnetic agglomeration of the δ-FeOOH particles, as discussed in the characterization section. The agglomeration resulted in a reduced contact area and blockage of some active sites, as evidenced in some similarly published works utilizing δ-FeOOH particles [21–22]. The composited δ-FeOOH/BC particles showed an improved performance of ~23% due to the increased contact surface area of δ-

FeOOH caused by dispersion on the BC surface. However, the removal efficiency was still relatively low. Overall, the removal efficiency of the catalysts ranged from approximately 12–23%, and the total removal rates did not significantly change between 10–30 min.

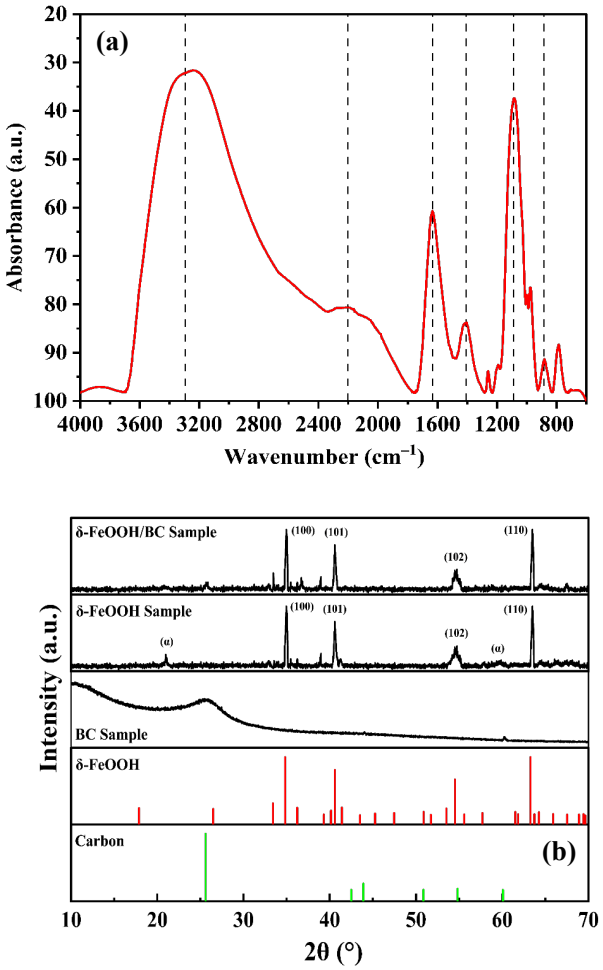

Figure 2 Infrared spectrum of (a) δ-FeOOH/BC composite and (b) X-ray diffractogram of the δ-FeOOH/BC composite.

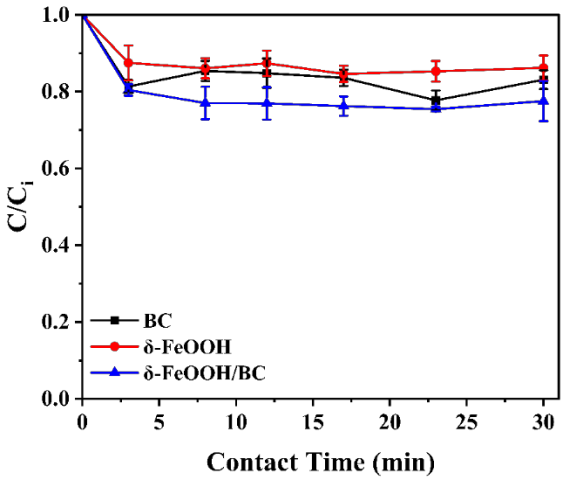

Figure 3 MB adsorption curves of the BC, δ-FeOOH, and δ-FeOOH/BC systems. Conditions: [MB]=30 mg L^{-1}; catalyst=0.250 g L^{-1}; pH=6.0; temp=25 °C; contact time =30 min.

As shown in Figure 4, the utilization of PMS alone resulted in only 5.51% removal of MB due to its low oxidation potential (E_0=1.77 V). As a consequence, inactivated PMS generates insufficient $SO_4^{\bullet-}$ radicals, which are responsible for oxidizing MB [23]. The BC/PMS system exhibited a noteworthy degradation performance of 41.59%. The enhanced removal could be attributed to the partial carbocatalytic activation of PMS by oxygenated functional groups (–OH and C=O) found on the surface of the synthesized BC [24]. The persistent free radicals formed from the decomposition of lignin bonds found in waste Pili nutshells during pyrolysis could also have contributed to the activation of PMS [25]. Although the removal of 51.12% slightly surpassed that of the BC/PMS system, δ-FeOOH alone could not fully activate PMS, possibly because of particle agglomeration, reducing the surface area in contact with PMS and MB.

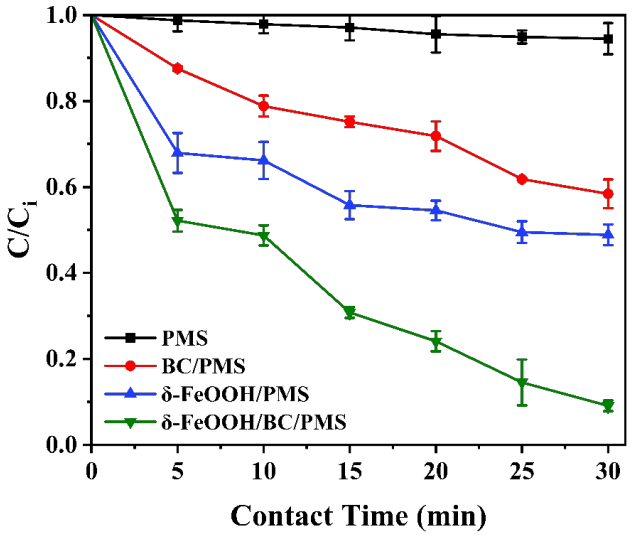

Figure 4. MB degradation curves of the BC, δ-FeOOH, and δ-FeOOH/BC systems. Conditions: [MB]=30 mg L^{-1}; [PMS]=0.4 g L^{-1}; catalyst=0.250 g L^{-1}; pH=6.0; temp=25 °C; contact time=30 min.

The highest removal of 90.88% was noted when the δ-FeOOH/BC/PMS system was used. This could be explained by the electron transfer reactions facilitated by the oxygenated functional groups of BC with PMS coupled with the highly porous structure of BC, which enabled the adhesion of δ-FeOOH. The δ-FeOOH synergistically enhanced the redox reaction with PMS, which led to the production of more highly reactive $SO_4^{\bullet-}$, as depicted by Eq. 6 [3]. Eventually, these reactive $SO_4^{\bullet-}$ radicals have the potential to mineralize MB, as reflected in Eq. 7.

$$Fe^{+2} + HSO_5^- \rightarrow SO_4^{\bullet-} + Fe^{+3} + OH^- \quad \text{(Eq. 6)}$$

$$MB + SO_4^{\bullet-} \rightarrow SO_4^{-2} + MB^{\bullet+} \quad \text{(Eq. 7)}$$

3) Degradation kinetics

The removal data obtained from batch degradation experiments were evaluated via pseudo-first-order and pseudo-second-order kinetic models previously given in Eqs. 4 and 5. The linearized plots were obtained by plotting the left-sind values of the equation versus contact time, as illustrated in Figure 5.

According to the obtained kinetic data shown in Table 1, the pseudo-first-order model appears to provide a better fit for the experimental data of all the treatment systems on the basis of the higher R^2 values. This implies that the MB concentration is the main factor limiting the rate of degradation and that the concentrations of PMS, δ-FeOOH, and BC are sufficiently high to have no discernible effect on the reaction rate. MB degradation following pseudo-first-order kinetics has also been reported in some PMS activation studies [26–28]. Moreover, a notable increase in the first-order kinetic constant was observed, increasing from 0.002 min^{-1} when PMS alone was used to 0.0782 min^{-1} for the δ-FeOOH/BC/PMS system. This significant enhancement suggests the synergistic effect of the combined system, resulting in an accelerated reaction rate of ~40 times compared to that of PMS.

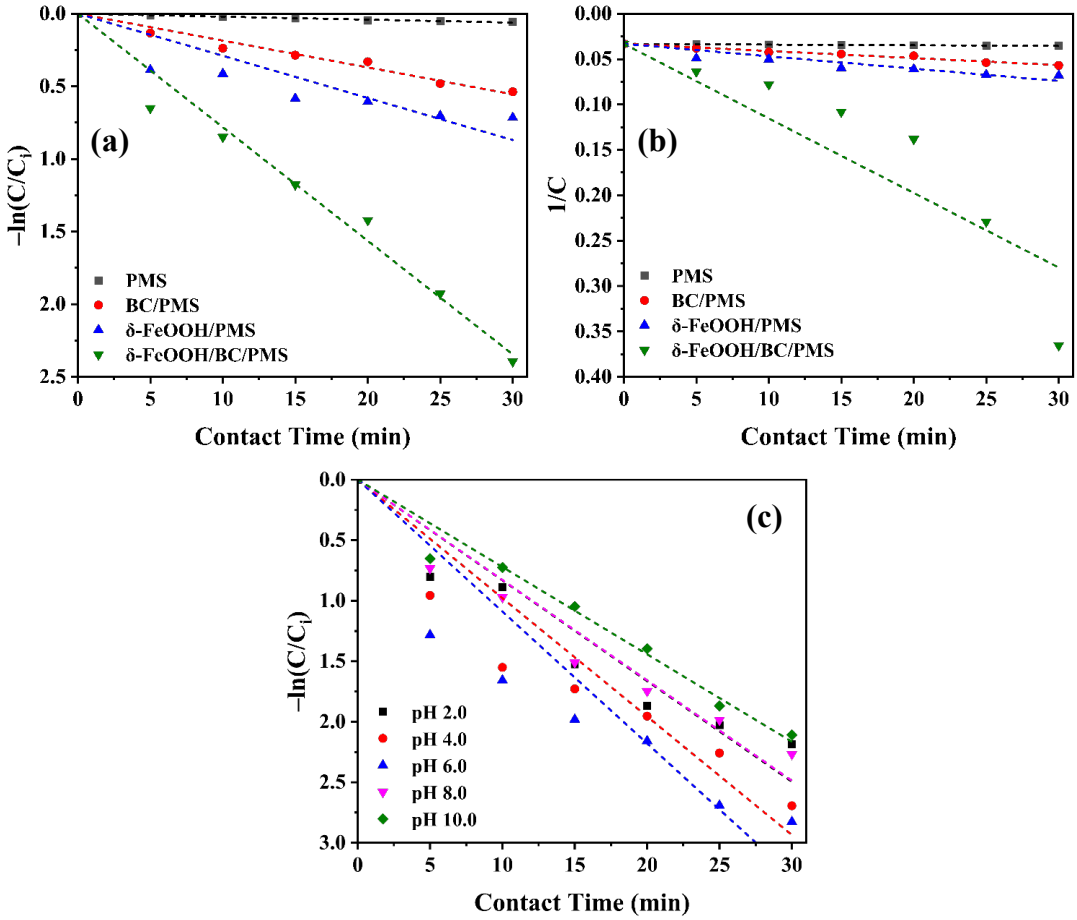

Figure 5 Plots of (a) MB degradation kinetics plotted using the pseudo-first-order type, (b) pseudo-second-order type, and (c) influence of different pH values on the pseudo-first-order kinetic parameters.
Conditions: [MB]=30 mg L^{-1}; [PMS]=0.4 g L^{-1}; catalyst=0.250 g L^{-1}; pH=6.0; temp=25 °C; contact time=30 min.

Table 1 Comparison of the kinetic parameters of MB removal by different treatment systems

Pseudo-first-order type			
Treatment system	**Kinetic equation**	**k_{obs} (min^{-1})**	**R^2**
PMS	$-\ln(C/C_i) = 0.0020t$	0.0020	0.9942
BC/PMS	$-\ln(C/C_i) = 0.0185t$	0.0185	0.9915
δ-FeOOH/PMS	$-\ln(C/C_i) = 0.0290t$	0.0290	0.9407
δ-FeOOH/BC/PMS	$-\ln(C/C_i) = 0.0782t$	0.0782	0.9932
Pseudo-second-order type			
Treatment system	**Kinetic equation**	**k_{obs} (L mg^{-1} min^{-1})**	**R^2**
PMS	$1/C = (7x10^{-5})t + 0.0333$	$7x10^{-5}$	0.9836
BC/PMS	$1/C = 0.0008t + 0.0333$	0.0008	0.9761
δ-FeOOH/PMS	$1/C = 0.0014t + 0.0333$	0.0014	0.9049
δ-FeOOH/BC/PMS	$1/C = 0.0082t + 0.0333$	0.0082	0.8523

The activity of the catalysts and reactants involved in the degradation process can be strongly impacted by the pH of the reaction environment. In this case, the changes in the kinetic parameters determined via the pseudo-first-order model were also investigated at different pH values. As shown in Table 2, the k_{obs} increased from 0.0832 min^{-1} to 0.1090 min^{-1} as the pH increased from 2.0–6.0, highlighting that degradation occurred more rapidly and efficiently under slightly acidic circumstances. Acid catalysis increases the production of Fe^{+2} ions from δ-FeOOH under acidic to nearly neutral conditions. Fe^{+2} ions may therefore combine with excess HSO_5^- to increase the formation of $^{\bullet}OH$ and $SO_4^{\bullet-}$ radicals to aid in MB degradation. Nevertheless, an oversupply of Fe^{+3} might cause radical scavenging of $SO_4^{\bullet-}$, which negatively affects the kinetic constant, as exhibited at pH 2.0 [29]. Additionally, under highly alkaline conditions, PMS could self-decompose, which lessens its ability to break down MB. For this reason, as the pH increased from 8.0–10.0, the kinetic rate constant dramatically decreased from 0.0829–0.0722 min^{-1}. Overall, the treatment system could be implemented over a wide pH range, which could result in lower operational expenses. While some advanced oxidation processes, such as the Fenton reaction, are extremely sensitive to pH, PMS-based treatments may work well in both basic and acidic environments, albeit with modest efficiency shifts.

4) Effect of catalyst dosage

The influence of catalyst dosage on MB removal is shown in Figure 6(a). Increasing the catalyst dosage from 0.050 g L^{-1} to 0.450 g L^{-1} resulted in an increase in the removal performance up to 98.46%. The additional loading of the catalyst in the system increased the number of catalytic active sites for PMS activation. It also increased the amount of Fe^{+2} dissolved in the solution, therefore leading to the formation of more $^{\bullet}OH$ and $SO_4^{\bullet-}$ radicals through Fe^{+2}/Fe^{+3} redox loops [29]. However, further increasing the catalyst dosage beyond 0.350 g L^{-1} no longer results in significant MB removal at a fixed PMS dosage. The amount of PMS in the solution limits the rate of MB decontamination. Thus, increasing the catalyst dosage beyond a certain threshold no longer increases $SO_4^{\bullet-}$ production.

Table 2 Kinetic parameters of MB removal via a pseudo-first-order model at various pH values

pH	Kinetic equation	k_{obs} (min^{-1})	R^2
2.0	$-\ln(C/C_i) = 0.0832t$	0.0832	0.9770
4.0	$-\ln(C/C_i) = 0.0979t$	0.0979	0.9685
6.0	$-\ln(C/C_i) = 0.1090t$	0.1090	0.9580
8.0	$-\ln(C/C_i) = 0.0829t$	0.0829	0.9839
10.0	$-\ln(C/C_i) = 0.0722t$	0.0722	0.9920

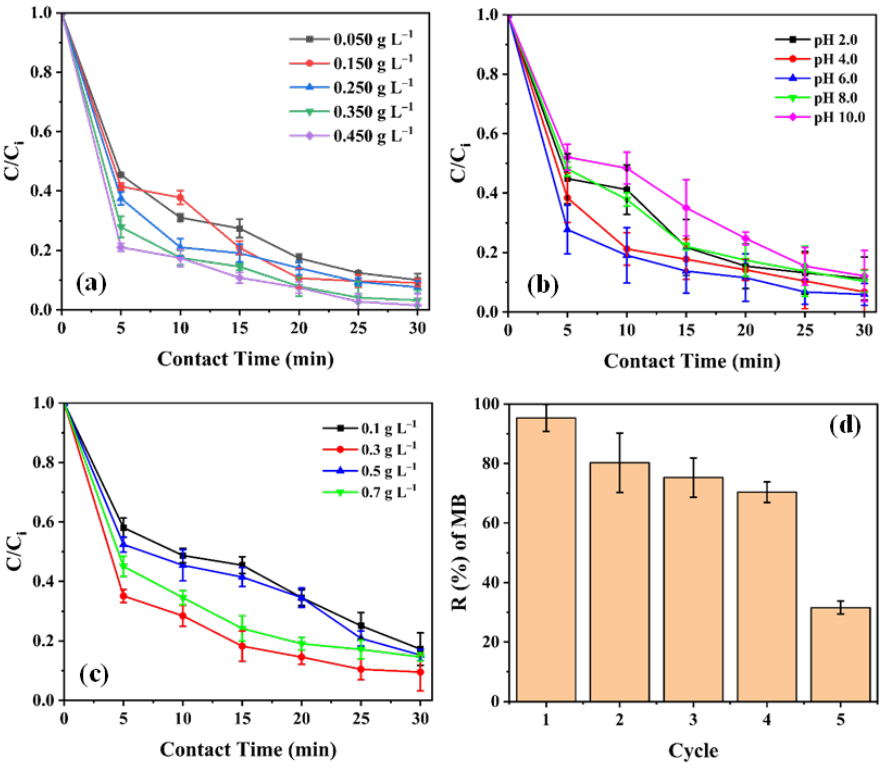

Figure 6 Plots showing (a) effect of catalyst addition on the degradation of MB, (b) effect of pH addition on the degradation of MB, (c) effect of PMS addition on the degradation of MB, and (d) recyclability performance of the composite. Conditions: [MB]=30 mg L^{-1}; [PMS]=0.3 g L^{-1}; catalyst=0.350 g L^{-1}; pH=6.0; contact time=30 min.

5) Effect of pH

Figure 6(b) shows the results of removal at different pH values. The performance was notably appreciable over a wide pH range (2.0–10.0), resulting in >85% removal. The optimal removal of 94.08% was attained in a slightly acidic environment at pH 6.0. Since the BC surface is mainly composed of negatively charged species, acidic conditions favor the formation of charged complexes on the surface of the catalyst [30]. In addition, acid catalysis increases the production of Fe^{+2} ions from δ-FeOOH. Consequently, Fe^{+2} ions could interact with excess HSO_5^-, leading to increased $^{\bullet}OH$ and $SO_4^{\bullet-}$ radical generation. However, an excessive amount of Fe^{+3} may result in radical scavenging of $SO_4^{\bullet-}$, which has a serious effect on MB degradation, as depicted at pH 2.0–4.0 [29].

$$Fe^{+2} + HSO_5^- \rightarrow Fe^{+3} + SO_4^{2-} + {}^{\bullet}OH \quad \text{(Eq. 8)}$$

$$Fe^{+2} + HSO_5^- \rightarrow SO_4^{\bullet-} + Fe^{+3} + OH^- \quad \text{(Eq. 9)}$$

The speciation of MB at different pH values may also have influenced the removal performance. Generally, the undissociated form of MB dominates at pH<pKa (pKa= 3.8). Beyond pH 6.0, cationic MB is practically the only species present in the solution. The neutral or undissociated form of MB is shown to be less polar and soluble in water. This in turn reduces the mineralization efficiency of $SO_4^{\bullet-}$ radicals. On the other hand, the minor improvement in the MB removal efficiency at pH 6 may be linked to the electrostatic attraction among the positively charged MB, the catalyst surface, and $SO_4^{\bullet-}$ radicals, leading to extensive degradation. However, under highly alkaline conditions, the generation of less powerful $^{\bullet}OH$ radicals could also be amplified. These $^{\bullet}OH$ radicals are also notable quenchers of $SO_4^{\bullet-}$, consequently decreasing the $SO_4^{\bullet-}$ concentration in the system, as reflected by a pH of 8.0–10.0 [31]. Similar behavior under alkaline conditions has been observed in several published studies utilizing PMS oxidants [3, 29].

$$SO_4^{\bullet-} + OH^- \rightarrow {}^{\bullet}OH + SO_4^{2-} \quad \text{(Eq. 10)}$$

$$SO_4^{\bullet-} + {}^{\bullet}OH \rightarrow SO_4^{2-} + H^+ + 0.5O_2 \quad \text{(Eq. 11)}$$

6) Effect of the PMS concentration

As shown in Figure 6(c), 0.3 g L^{-1} PMS resulted in the highest MB removal of 90.47%. Further loading of PMS into the solution resulted in decreased removal performance. Excess HSO_5^- in the solution could scavenge $^{\bullet}OH$ and $SO_4^{\bullet-}$ radicals, leading to a decrease in the removal ability of the system, as given by Eqs. 12 and 13 [31]. The percentage of MB removal was also low at low PMS dosages because of limited radical generation. A plausible explanation for this could be the limitation of the catalyst's active sites, which hinder the catalytic activity of the material [32].

$$SO_4^{\bullet-} + HSO_5^- \rightarrow HSO_4^- + SO_5^{\bullet-} \quad \text{(Eq. 12)}$$

$$^{\bullet}OH + HSO_5^- \rightarrow H_2O + SO_5^{\bullet-} \quad \text{(Eq. 13)}$$

7) Recyclability and radical quenching experiments

For large-scale applications of this technology, efficient catalyst reuse can reduce overall treatment costs, limit waste generation, and lower energy inputs. Recyclability tests were conducted to assess the catalytic activity and stability of the composite upon repeated use. The catalyst was filtered, washed, and subsequently recycled for another four runs following the optimized conditions. Figure 6(d) shows that after four consecutive cycles, the removal efficiency remained relatively high (>70.00%). Over five cycles, the removal decreased from 95.31% to 40.26%. The decrease in its catalytic activity could be due to the unavoidable loss of δ-FeOOH during the catalytic reaction, leading to a decrease in the number of binding sites on the surface. As presented earlier, Fe^{+2}/Fe^{+3} from δ-FeOOH provides the driving force for $SO_4^{\bullet-}$ generation. Leaching of δ-FeOOH particles might also have occurred due to multiple washes, restricting the production of $SO_4^{\bullet-}$. Other possible causes could include the collapse and fouling of the catalyst surface due to the formation of byproducts and the occupation of active sites by MB.

Simple radical scavenging experiments were carried out to determine the dominant radicals responsible for MB degradation. Figure 7 shows that MB removal was significantly reduced in the presence of both $(CH_3)_3COH$ and C_2H_5OH as probe reagents. $(CH_3)_3COH$ quenches primarily $^{\bullet}OH$ radicals, whereas C_2H_5OH scavenges both $^{\bullet}OH$ and $SO_4^{\bullet-}$ radicals [33]. The quenching mechanisms can be represented by Eqs. 14–16.

$$^{\bullet}OH + (CH_3)_3COH \rightarrow {}^{\bullet}(CH_3)_3CO + H_2O \quad \text{(Eq. 14)}$$

$$^{\bullet}OH + C_2H_5OH \rightarrow {}^{\bullet}C_2H_5O + H_2O \quad \text{(Eq. 15)}$$

$$SO_4^{\bullet-} + C_2H_5OH \rightarrow {}^{\bullet}C_2H_5O + HSO_4^- \quad \text{(Eq. 16)}$$

The quenching effect of C_2H_5OH (~20% removal) was stronger than that of $(CH_3)_3COH$ (~50% removal), indicating that $SO_4^{\bullet-}$ radicals played a dominant role as the main reactive species responsible for MB degradation. Even so, a more comprehensive radical inhibition experiment should be performed taking into account other possible reactive species, such as h^+, $O_2^{\bullet-}$, and $^1O_2$, to elucidate possible pathways and reaction mechanisms for MB degradation. Trapping agents such as potassium iodide, 1,4-benzoquinone, and sodium azide can be used to trap h^+, $O_2^{\bullet-}$, and $^1O_2$, respectively.

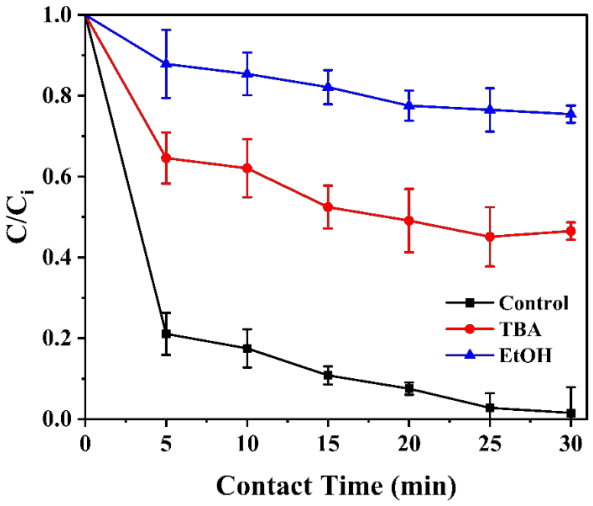

Figure 7 Results of radical quenching experiments using $(CH_3)_3COH$ and C_2H_5OH. Control: [MB]=30 mg L^{-1}; [PMS]=0.3 g L^{-1}; catalyst=0.350 g L^{-1}; pH=6.0; temp=25 °C; contact time=30 min.

Conclusion and recommendations

The oxidative removal of MB dye via the δ-FeOOH/BC/PMS system was carried out in this study and showed promising application potential in the field of advanced wastewater treatment. Characterization techniques confirmed successful composite preparation. Comparative catalytic degradation experiments revealed 90.88% MB removal after 30 min using 0.4 g L^{-1} PMS and 0.25 g L^{-1} catalyst at pH 6.0. The impregnation of δ-FeOOH particles onto BC catalyzed the formation of Fe^{+2}, which eventually improved the formation of $SO_4^{\bullet-}$ responsible for MB removal. Process conditions such as pH, catalyst dosage, and initial PMS concentration significantly influenced the removal performance of the δ-FeOOH/BC/PMS system. The maximum removal was 98.46% when 0.45 g L^{-1} catalyst was used, 94.08% when pH 6.0 was used, and 90.47% when 0.3 g L^{-1} PMS was used. Overall, the treatment system could be used at a wide range of pH values, which is beneficial for wastewater with various pH characteristics. In addition, a balance between the catalyst dosage and PMS dosage was crucial for optimal performance. Recyclability tests revealed >70% removal even after four treatment cycles, indicating the composite's ability to maintain its catalytic ability. Moreover, radical quenching experiments revealed that $SO_4^{\bullet-}$ with minor contributions from $^{\bullet}OH$ radicals, was the radical responsible for MB mineralization. Further research on other process parameters (e.g., detailed reaction kinetics, thermodynamics, effects of water matrices, and the effect of Fe:BC mass ratio) is recommended. Economic and life cycle analyses of the material should also be comprehensively performed, especially for future large-scale production.

References

[1] Cwalinski, T., Polom, W., Marano, L., Roviello, G., D'Angelo, A., Cwalina, N., …, Polom, K. Methylene blue—current knowledge, fluorescent properties, and its future use. Journal of Clinical Medicine, 2020, 9(11), 3538.

[2] Li, X., Jie, B., Lin, H., Deng, Z., Qian, J., Yang, Y., Zhang, X. Application of sulfate radicals-based advanced oxidation technology in degradation of trace organic contaminants (TrOCs): Recent advances and prospects. Journal of Environmental Management, 2022, 308, 114664.

[3] Fan, J., Zhao, Z., Ding, Z., Liu, J. Synthesis of different crystallographic FeOOH catalysts for peroxymonosulfate activation towards organic matter degradation. RSC advances, 2018, 8(13), 7269–7279.

[4] Zhou, Y., Zhou, S., Yi, M., Li, Y., Shang, J., Cheng, X. Enhanced peroxymonosulfate activation for organic decontamination by Ni-doped δ-FeOOH under visible-light assistance. Environmental Research, 2025, 265, 120472.

[5] Gęca, M., Wiśniewska, M., Nowicki, P. Biochars and activated carbons as adsorbents of inorganic and organic compounds from multicomponent systems–A review. Advances in Colloid and Interface Science, 2022, 102687.

[6] Lirag, T.B., Foronda, V.R., Ativo, A.O., Estrella, M.N. Demographic evaluation of Pili farmers and their production capacity in Bicol Region, Philippines. Asian Journal of Agricultural Extension, Economics & Sociology, 2023, 41(1), 15–25.

[7] Millena, C.G., Baloloy, K.A.V., Doma, N.G., Hernan, P.B. Effect of maturity on physicochemical and fatty acid profile of Philippine Pili (Canarium ovatum Engl.). Philippine Journal of Science, 2023, 152(1), 159–171.

[8] Prado, J.A., Brillante, F.D., Mendez, J.C.B., Ocampo, D.M. Utilization of Pili (*Canarium Ovatum*) sawdust in the production of bio-crude oil and identification of its potential byproducts using thermochemical conversion. International Journal of Chemical and Biochemical Sciences, 2024, 25(19), 1115–1121.

[9] Jeníček, L., Tunklová, B., Malaťák, J., Velebil, J., Malaťáková, J., Neškudla, N., Hnilička, F. The impact of nutshell biochar on the environment as an alternative fuel or as a soil amendment. Materials, 2023, 16(5), 2074.

[10] Yao, M.G., Pondevida, J.L., Cheng, C.F., Camacho, D.H. Enhancement of CO_2 adsorption on activated carbon prepared from Canarium ovatum Engl. Nut Shells. Philippine Journal of Science, 2015, 144(2), 149–159.

[11] Threepanich, A., Praipipat, P. Powdered and beaded lemon peels-doped iron (III) oxide-hydroxide materials

for lead removal applications: Synthesis, characterizations, and lead adsorp-tion studies. Journal of Environmental Chemical Engineering, 2021. 9(5), 106007.

[12] Mei, L., Liao, L., Wang, Z., Xu, C. Interactions between phosphoric/tannic acid and different forms of FeOOH. Advances in Materials Science and Engineering, 2015, 250836.

[13] Nasrazadani, S., Hassani, S. Modern analytical techniques in failure analysis of aerospace, chemical, and oil and gas industries. Handbook of Materials Failure Analysis with Case Studies from the Oil and Gas Industry, 2016, 39–54.

[14] Zeng, B., Xu, W., Khan, S.B., Wang, Y., Zhang, J., Yang, J., …, Lin, Z. Preparation of sludge biochar rich in carboxyl/hydroxyl groups by quenching process and its excellent adsorption performance for Cr (VI). Chemosphere, 2021. 285, 131439.

[15] Yang, F., Zhang, S., Li, H., Li, S., Cheng, K., Li, J-S., Tsang, D.C.W. Corn straw-derived biochar impregnated with α-FeOOH nanorods for highly effective copper removal. Chemical Engineering Journal, 2018, 348, 191–201.

[16] Saleh, M.E., Mahmoud, A.H., Rashad, M. Biochar usage as a cost-effective bio-sorbent for removing NH_4-N from wastewater. in The international conference the Global Climate Change, Biodiversity and Sustainability: Challenges and Opportunities in Arab MENA region and EuroMed, 2013.

[17] Zhang, L., Li, H., Yang, B., Han, N., Wang, Y., Zhang, Z., …, Gao, Y. Promote the electrocatalysis activity of amorphous FeOOH to oxygen evolution reaction by coupling with ZnO nanorod array. Journal of Solid State Electrochemistry, 2020, 24(4), 905–914.

[18] Wyckoff, R., American Mineralogist Crystal Structure Database. 1963.

[19] Destyorini, F., Irmawati, Y., Hardiansyah, A., Widodo, H., Yahya, I.N.D., Indayaningsih, N., …, Uyama, H. Formation of nanostructured graphitic carbon from coconut waste via low-temperature catalytic graphitisation. Engineering Science and Technology, an International Journal, 2021, 24(2), 514–523.

[20] Tavares, T.S., da Rocha, E.P., Nogueira, F.G.E., Torres, J.A., Silva, M.C., Kuca, K., Ramalho, T.C., Δ-FeOOH as support for immobilization peroxidase: optimization via a chemometric approach. Molecules, 2020, 25(2), 259.

[21] Lin, Z., Huan, Z., Zhang, J., Li, J., Li, Z., Guo, P., …, Zhang, T. CTAB-functionalized δ-FeOOH for the simultaneous removal of arsenate and phenylarsonic acid in phenylarsenic chemical warfare. Chemosphere, 2022, 292, 133373.

[22] Zhao, L., Zhang, H., Zhao, B., Lyu, H. Activation of peroxydisulfate by ball-milled α-FeOOH/biochar composite for phenol removal: Component contribution and internal mechanisms. Environmental Pollution, 2022, 293, 118596.

[23] Xiao, R., Luo, Z., Wei, Z., Luo, S., Spinney, R., Yang, W., Dionysiou, D.D. Activation of peroxymonosulfate/persulfate by nanomaterials for sulfate radical-based advanced oxidation technologies. Current Opinion in Chemical Engineering, 2018, 19, 51–58.

[24] Xu, L., Wu, C., Liu, P., Bai, X., Du, X., Jin, P., …, Wang, Y. Peroxymonosulfate activation by nitrogen-doped biochar from sawdust for the efficient degradation of organic pollutants. Chemical Engineering Journal, 2020, 387, 124065.

[25] Zhang, C., Wang, Z., Li, F., Wang, J., Xu, N., Jia, Y., …, Shen, W. Degradation of tetracycline by activated peroxodisulfate using $CuFe_2O_4$-loaded biochar. Journal of Molecular Liquids, 2022, 368, 120622.

[26] Li, J., Xu, M., Yao, G., Lai, B. Enhancement of the degradation of atrazine through $CoFe_2O_4$ activated peroxymonosulfate (PMS) process: kinetic, degradation intermediates, and toxicity evaluation. Chemical Engineering Journal, 2018, 348, 1012–1024.

[27] Wang, S., Wang, J. Synergistic effect of PMS activation by Fe^0@Fe_3O_4 anchored on N, S, O co-doped carbon composite for degradation of sulfamethoxazole. Chemical Engineering Journal, 2022, 427, 131960.

[28] He, B., Song, L., Zhao, Z., Liu, W., Zhou, Y., Shang, J., Cheng, X. $CuFe_2O_4$/CuO magnetic nanocomposite activates PMS to remove ciprofloxacin: Ecotoxicity and DFT calculation. Chemical Engineering Journal, 2022, 446, 137183.

[29] Jiang, S.F., Ling, L.L., Chen, W.-J., Liu, W.J., Ji, D.C., Jiang, H. High efficient removal of bisphenol A in a peroxymonosulfate/iron func-tionalized biochar system: Mechanistic elucidation and quantifycation of the contributors. Chemical Engineering Journal, 2019, 359, 572–583.

[30] Devi, L.G., Srinivas, M., ArunaKumari, M. Heterogeneous advanced photo-Fenton process using peroxymonosulfate and peroxydisulfate in presence of zero valent metallic iron: A comparative study with hydrogen peroxide photo-Fenton process. Journal of Water Process Engineering, 2016, 13, 117–126.

[31] Crincoli, K.R., Green, C., Huling, S.G. Sulfate radical scavenging by mineral surfaces in persulfate-driven oxidation systems: reaction rate constants and implications. Environmental Science & Technology, 2020, 54(3), 1955–1962.

[32] Huang, W., Tang, Y., Zhang, X., Luo, Z., Zhang, J. nZVI-biochar derived from Fe_3O_4-loaded rabbit manure for activation of peroxymono-sulfate to degrade sulfamethoxazole. Journal of Water Process Engineering, 2022, 45, 102470.

[33] Lei, Y., Yu, Y., Lei, X., Liang, X., Cheng, S.S. Ouyang, G., Yang, X. Assessing the use of probes and quenchers for understanding the reactive species in advanced oxidation processes. Environmental Science & Technology, 2023, 57(13), 5433–5444.